Title

Mutual neutralization in collisions of H+ with Cl−

Journal

The Journal of Chemical Physics, 151(21)

ISSN

0021-9606

Authors

Larson, Åsa
Hörnquist, Johan
Hedvall, Patrik
et al.

Publication Date

2019-12-07

DOI

10.1063/1.5128357

Peer reviewed

Mutual neutralization in collisions of H^+ with Cl^-

Åsa Larson*,[1] Johan Hörnquist,[1] Patrik Hedvall,[1] and Ann E. Orel[2]

[1]*Department of Physics, Stockholm University, AlbaNova University Center, S-106 91 Stockholm, Sweden*

[2]*Department of Chemical Engineering, University of California, Davis Davis, CA 95616, USA*

(Dated: November 6, 2019)

The cross section and final state distribution for mutual neutralization in collisions of H^+ with Cl^- have been calculated using an *ab initio* quantum mechanical approach. It is based on potential energy curves and non-adiabatic coupling elements for the six lowest $^1\Sigma^+$ states of HCl computed with the multi-reference configuration interaction method. The reaction is found to be driven by non-adiabatic interactions occurring at relatively small internuclear distances ($R < 6$ a_0). Effects on the mutual neutralization cross section with respect to the asymptotic form of the potential energy curves, inclusion of closed channels as well as isotopic substitution are investigated. The effect of spin-orbit interaction is investigated using a semi-empirical model and found to be small. A simple two-state Landau-Zener calculation fails to predict the cross section.

PACS numbers:

I. INTRODUCTION

Mutual neutralization is the process where oppositely charged ions collide and as a result of electron transfer, neutral fragments are formed. For an *ab initio* description of the reaction, the potential energy curves of the ionic and covalent states of the reaction complex must be computed as well as the corresponding non-adiabatic coupling elements. The process is in general driven by non-adiabatic couplings arising due to avoided crossings between ionic and covalent states occurring at large internuclear distances. In many cases highly excited electronic states are involved.

Ab initio and fully quantum mechanical studies of mutual neutralization reactions are so far limited to collisions of atomic ions. The studies include collisions of H^- with H^+ [1–3], He^+ [4], Li^+[5], Na^+ [6], Mg^+[7, 8] as well as F^- colliding with H^+ [9] and Li^+ [10, 11]. In the past there have been numerous studies of mutual neutralization reactions where the nuclear motion is described classically and the transition probabilities are estimated using e.g. the Landau-Zener model [12, 13]. There are several studies [3, 6, 7, 14, 15] where the cross sections obtained using the semi-classical model are compared with the ones calculated quantum mechanically. Provided the mutual neutralization reaction is driven by well-isolated avoided crossings occurring at large internuclear distances, the semi-classical model works well [15].

In the present study, mutual neutralization in collisions of H^+ and Cl^- is investigated using an *ab intio* fully quantum mechanical approach. At low collision energies the reaction:

$$H^+ + Cl^- \rightarrow H + Cl$$

can only form ground state fragments. A collision energy of about 0.21 eV is needed to form $H(n = 2)$+Cl. This system is interesting since the mutual neutralization reaction is driven by non-adiabatic interactions between lower lying states of $^1\Sigma^+$ symmetry occurring at small internuclear distances. In addition, there are strong interactions between valence, Rydberg and ionic states [16] that have not been present in other systems studied.

We have performed multi-reference configuration interaction calculations of the adiabatic potential energy curves and non-adiabatic couplings. The mutual neutralization reaction is studied by numerically solving the nuclear radial Schrödinger equation in a strict diabatic representation. We investigate the effect of inclusion of higher lying channels that are closed at low collision energies. The importance of spin-orbit interaction in the HCl system is investigated using a semi-empirical model [17, 18], where the spin-orbit Hamiltonian is derived using atomic spin-orbit parameters of the Cl atom. The cross sections, final state distributions and thermal rate constants for mutual neutralization are computed for collisions of H^+ with Cl^- as well as D^+ with Cl^-. Compared with other mutual neutralization reactions [3, 4] we find a different trend in the scaling of the mutual neutralization cross sections with the reduced mass of the collision complex. In addition, although only one state is open and the system appears to only involve a broad crossing between the ground and ion-pair state, the two-state Landau-Zener model fails completely. The cause of this failure is discussed and the importance of multi-state interactions is demonstrated.

At Stockholm University there is a cryogenic double electrostatic storage ring (DESIREE) constructed [19] to study collisions between oppositely charged atomic and/or molecular ions in well defined quantum states. Experimental studies of mutual neutralization reactions have also been based on single-pass merged-beam experiments [20–22] or flowing afterglow-Langmuir probe mea-

*Corresponding author; e-mail: aasal@fysik.su.se

surements [23, 24]. In a recent study [24], the mutual neutralization rate constants for the reactions of H^+ and D^+ with the atomic halide anions Cl^-, Br^- and I^- was measured at room temperature (300 K) using a flowing afterglow Langmuir probe apparatus. Our calculated rates are compared with the measured ones for the $H^+/D^+ + Cl^-$ reactions. It should be noted that these experiments measured the disappearance of the cation. Associative ionization, the process $H^+ + Cl^- \rightarrow HCl^+ + e^-$ would be counted as mutual neutralization. Therefore, direct comparison between theory and experiment assumes the cross section for associative ionization is small.

The article is organized as follows. Section II describes how the relevant potential energy curves and couplings of the HCl are computed. Section III briefly describes the diabatization of the electronic states and how the coupled Schrödinger equation for the nuclear motion is solved. In this section, the method of including the spin-orbit interaction is outlined. Further, the method of including the spin-orbit interaction is outlined and the calculation of the rate constant is discussed. Finally in section IV, the calculated total mutual neutralization cross section and final state distributions are displayed. Effects from isotopic substitution, inclusion of couplings to higher lying electronic states are discussed as well as the comparisons to the semi-classical calculation and the measured rate constants are presented. Throughout the article, atomic units are used.

II. POTENTIAL ENERGY CURVES AND COUPLINGS

We compute adiabatic potential energy curves and non-adiabatic interactions among the six lowest electronic states of $^1\Sigma^+$ symmetry of HCl. The first excited state of this symmetry is asymptotically associated with the ion-pair $H^+ + Cl^-$ limit, while the other states are covalent states dissociating into neutral fragments. At small internuclear distances, the excited covalent states are Rydberg states with an ionic core corresponding to the HCl^+ $X^2\Pi$ ground state. Our previous study on dissociative recombination of HCl^+[25] reveals that there are interactions between the Rydberg states converging to the ground ionic core with families of Rydberg states converging to the excited ionic cores. To obtain an accurate and balanced description of these series of Rydberg states, molecular orbitals obtained from a state-averaged calculation on the two lowest electronic states of the ion are used in the subsequent calculation on the neutral molecular system. These ionic molecular orbitals are used instead of the molecular orbitals of the ground state of the neutral molecule since they will provide a better description of the Rydberg states and hence avoid an over-correlation of the HCl ground state.

All structure calculations are carried out using the MESA program package [26]. The calculations start with a Hartree-Fock calculation on the ground state of the HCl^+ ion ($X^2\Pi$) using a contracted (14s8p4d/11s7p3d) basis set for H and a (13s11p3d/6s6p3d) basis set given by McLean [27] for Cl, augmented with the addition of (4s,3p,2d) functions centered on the chlorine atom. These Hartree-Fock orbitals are then used as a basis for a multi-reference configuration interaction (MRCI) calculation on the HCl^+ ion to determine the natural orbitals. The MRCI wave function included all single and double excitations out of the reference configurations generated when the lowest five orbitals are doubly occupied and the remaining seven electrons are excited among five orbitals; 4σ, 5σ, 6σ, $2\pi_x$ and $2\pi_y$. The natural orbitals averaged over the three lowest ion states (the two degenerate components of the $X^2\Pi$ state and the next $A^2\Sigma^+$ state) are obtained.

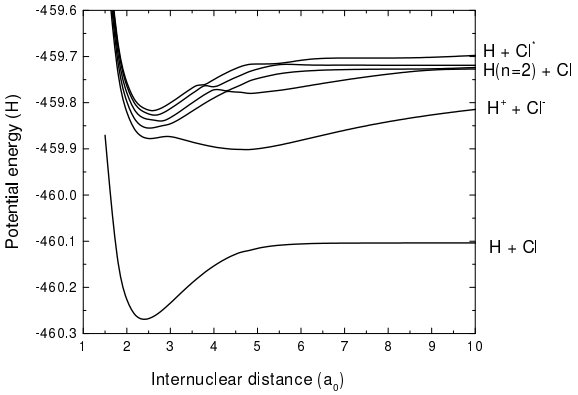

FIG. 1: Adiabatic potential energy curves of HCl in $^1\Sigma^+$ symmetry.

These natural orbitals are then used as input to a state-averaged complete active space self-consistent-field (CASSCF) calculation on the ground and first excited states of the ion, which is carried out in no symmetry. The CASSCF orbitals are required in the MESA program when non-adiabatic couplings are computed. In this calculation the lowest five orbitals are doubly occupied and the active space includes the following five orbitals and seven electrons. These orbitals are used in the final MRCI calculation on the HCl system, where the first five orbitals are frozen and the reference configurations are generated by allowing for excitations of the eight electrons among the next five orbitals. Single external excitations out of the reference configurations are included.

Figure 1 shows the calculated adiabatic potential curves in the range 1.0 a_0 to 10 a_0. The first excited state in this symmetry, $2^1\Sigma^+$, correlates with the $H^+ + Cl^-$ ion-pair limit. This state has the characteristic double well potential seen in other studies [16, 28–30]. The shape of the potentials and the location of the avoided crossings largely agrees with previous studies [16, 28–30]. All avoided crossings occur at relatively small internu-

clear distances ($R < 6$ a$_0$). There are avoided crossing at internuclear distances 2.5 a$_0$ $< R <$ 3.0 a$_0$ and in the region 4.0 a$_0$ $< R <$ 5.0 a$_0$. In these regions, the Rydberg states converging to the ground state of the ion are crossed by dissociative states. At small internuclear distances these dissociative states are embedded in the ionization continuum and are electronic resonant states. The states are important for the direct electron capture in dissociative recombination of HCl^+ [25]. In present study, however, only bound electronic states are considered.

The adiabatic potential energy curves are extrapolated from 15 a$_0$ to large internuclear distances to obtain the theoretical asymptotic energies. The covalent states are assumed to be constant, while the ion-pair has the form:

$$V(R) = V_{th} - \frac{1}{R} - \frac{\alpha}{2R^4} \qquad (1)$$

where $\alpha = 27.14$ au is the polarizability of Cl^- [31] and V_{th} is the asymptotic value of the ion-pair potential. Table I lists all six states included in the calculation, as well as the experimental [32] and calculated asymptotic energy limits relative to the energy of the ground state fragments. Extrapolating the ion-pair ($2^1\Sigma^+$) potential

TABLE I: Asymptotic limits of the six lowest $^1\Sigma^+$ states of HCl.

State	Asymptotic limit	Experimental energy [32]	Calculated energy
$X^1\Sigma^+$	H($n=1$)+Cl($3p^5\ ^2P$)	0	0
$2^1\Sigma^+$	H^++Cl^-	9.99	10.63
$3^1\Sigma^+$	H($n=2$)+Cl($3p^5\ ^2P$)	10.20	10.25
$4^1\Sigma^+$	H($n=2$)+Cl($3p^5\ ^2P$)	10.20	10.43
$5^1\Sigma^+$	H($n=2$)+Cl($3p^5\ ^2P$)	10.20	10.47
$6^1\Sigma^+$	H($n=1$)+Cl($3p^4 4s^1\ ^2D$)	10.43	11.42

to large distances provides an asymptotic energy that lies above the energy of the states (3 - 5)$^1\Sigma^+$, which does not agree with the experimental data [32]. The potential of the ion-pair state is in general more challenging to accurately compute than the low lying covalent states. The dissociation of the highest lying state $6^1\Sigma^+$ is not as well described due to the less accurate description of the excited states of Cl.

To evaluate the quality of the adiabatic potential energy curves, a comparison with previous theoretical studies as well as experimental data have been made. Figure 2 shows a comparison with potentials computed by Engin *et al.* [30]. They performed *ab initio* configuration interactions calculations including up to quadruple electronic excitations (CI-SDTQ) of a variety of low-lying states of HCl, where the ground state and first three excited states of $^1\Sigma^+$ symmetry were included. In Fig. 2, the potentials have been shifted in order for the minimum energy of the ground state to agree. The energies of the potentials of [30] all lie higher than the present study, with the ground state having a difference of about 0.04 H or 1.1 eV at the minimum. Of more importance for the

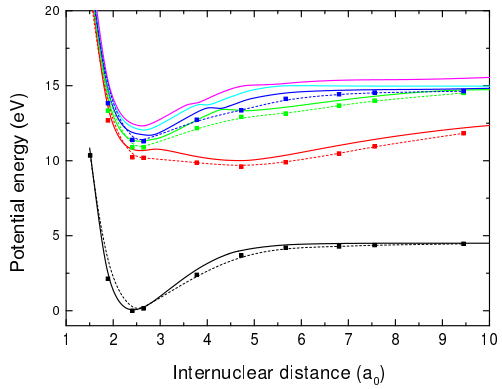

FIG. 2: (Color online) Adiabatic potential energy curves of $^1\Sigma^+$ symmetry calculated here (solid) are compared with those computed by Engin *et al.* [30] (dashed lines with symbols).

mutual neutralization cross section are the relative energy differences between the ground state and the excited states. Table II shows the vertical excitation energies of states $X^1\Sigma^+$ and (2 - 4)$^1\Sigma^+$ at the equilibrium distance in comparison to other calculations [28–30]. In the present

TABLE II: Vertical excitation energies in eV obtained at the fixed internuclear distance R_e.

calculation	$2^1\Sigma^+$	$3^1\Sigma^+$	$4^1\Sigma^+$	R_e (Å)
Present study	10.71	11.32	11.85	1.270
Engin *et al.* [30]	10.23	10.89	11.39	1.275
Bettendorf *et al.* [29]	10.08	10.87	12.25	1.270
Hirst & Guest [28]	10.17	11.09	-	1.275

study, the first three excited states all lie higher relative the ground state, than those of Engin *et al.* [30]. A comparison of the spectroscopic data of the ground state $X^1\Sigma^+$ to a few other theoretical studies as well as with experimental data is summarized in Table III. We compare the dissociation energy D_0, first and second terms of the vibrational constants (ω_e and $\omega_e x_e$) as well as the equilibrium bond length R_e. The spectroscopic data of

TABLE III: Comparison of molecular constants of the $X^1\Sigma^+$ state of HCl.

	D_0 (eV)	ω_e (cm^{-1})	$\omega_e x_e$ (cm^{-1})	R_e (Å)
Present study	4.33	2970	58.1	1.27
Engin *et al.* [30]	4.29	2770	-	1.29
Bettendorff *et al.* [29]	4.16	2960	-	1.28
Hirst & Guest [28]	4.05	3010	50.7	1.29
Experimental [33]	4.43	2990	52.8	1.28

the HCl electronic ground state are in good agreement with experimental data.

Using the MRCI wavefunctions, the non-adiabatic couplings are calculated analytically as described in [34, 35].

These coupling elements are derived from analytical gradient methods [35] and require the use of CASSCF orbitals. The analytical coupling elements have the advantage that they avoid the approximations applied when using finite difference methods or when couplings are obtained using the Hellmann-Feynman [36, 37] or Sidis [38] relations that are valid only for exact wave functions. Figure 3 shows the non-adiabatic coupling elements ($f_{ij} = \langle \Phi_i | \partial_R | \Phi_j \rangle$) between the ground state and four lowest excited $^1\Sigma^+$ states of HCl.

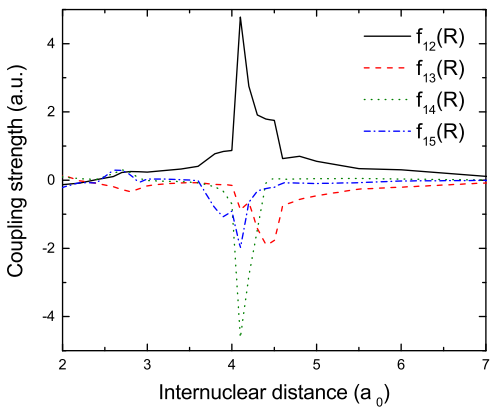

FIG. 3: Non-adiabatic first derivative coupling elements between the ground and excited $^1\Sigma^+$ states of HCl.

The non-adiabatic coupling between the two lowest adiabatic states extends over a significant range of internuclear distances, which is in agreement with the broad interaction region seen by the avoided crossing observed in the potential energy curves. However, there are also avoided crossings among the excited states in the region $[2.5, 3.0]$ a_0 and $[4.0, 5.0]$ a_0 where the Rydberg states interact with higher lying dissociative states. The adiabatic wave functions will change character in these regions and as a result there will be significant non-adiabatic coupling elements. All coupling elements among the six lowest $^1\Sigma^+$ states are computed and similar behavior is noted. The calculated non-adiabatic coupling elements as well as the adiabatic potential energy curves, are available as supplemental material.

III. DYNAMICS

The adiabatic potential energy curves are transformed to a strict diabatic representation by assuming that only a finite number ($N \leq 6$) of bound $^1\Sigma^+$ states are coupled. The orthogonal transformation matrix ($\mathbf{T}$) that transforms between the adiabatic and diabatic basis is obtained by numerically integrating the equation [39–41]

$$\frac{d}{dR}\mathbf{T} + \mathbf{fT} = \mathbf{0}, \tag{2}$$

where $\mathbf{f}$ is the anti-symmetric matrix containing the non-adiabatic first derivative coupling elements. At large internuclear distances, all non-adiabatic coupling elements are assumed to be zero and the asymptotic transformation matrix is an identity matrix.

Due to the presence of the Cl atom in the system, there is spin-orbit interaction that couples states of $^1\Sigma^+$ symmetry to electronic states of different symmetries. Using the MESA structure program [26] these spin orbit interactions can not be calculated *ab initio*. Instead, the spin-orbit interaction has been treated using a semi-empirical method [17, 18] where the spin-orbit coupling elements are obtained from the separated atom limit and are assumed to be independent of the internuclear distance. A spin-orbit coupling parameter corresponding to a splitting of 0.1094 eV [42] of the the $^2P_{1/2}$ and $^2P_{3/2}$ levels of Cl is used. The molecular spin-orbit Hamiltonian can then be derived by transforming from the atomic to molecular basis for the separated atoms. For electronic states with $\Omega = 0$, the spin-orbit interaction will couple singlet and triplet states of different symmetries. These adiabatic potentials have all been computed *ab initio*. The present model neglects all non-adiabatic interactions among other states than those of $^1\Sigma^+$ symmetry and it assumes that only states associated with the same asymptotic limit are coupled by the spin-orbit interaction.

The diabatic potential matrix is obtained by the similarity transformation $\mathbf{V}^d = \mathbf{T}^t \mathbf{V}^{ad} \mathbf{T}$ of the adiabatic potential matrix. By a partial wave expansion, the radial coupled Schrödinger equation in the diabatic representation is obtained. This equation is solved by numerically integrating the matrix Riccati equation for the logarithmic derivative of the radial wave function using Johnson's log-derivative method [43]. Details on the numerical procedure can be found in [2]. The scattering matrix, $S_{ij,l}$, is obtained by matching the logarithmic derivative of the radial wave function to the appropriate asymptotic solutions of the open or closed covalent or ionic channels, respectively. From the open-channel portion of the scattering matrix, the cross section for scattering from channel i to channel j is given by

$$\sigma_{ij}(E) = \frac{\pi}{k_i^2} \sum_{l=0}^{\infty} (2l+1) \left| S_{ij,l} - \delta_{ij} \right|^2 . \tag{3}$$

The mutual neutralization cross section is calculated for energies ranging from 0.001 to 10 eV. The matrix Riccati equation is solved numerically from 1.5 a_0 to 15 a_0 with an integration step size of 0.005 a_0. The total mutual neutralization cross section is then obtained by summing all contributions from the partial waves according to equation (3). The summation is terminated when the ratios of the partial cross sections and the accumulated integral cross sections remain less than 10^{-5} for 25 terms in succession. The number of partial waves that are included in the calculations ranged from around 150 for a collision energy of 1 meV to around 250 for a collision energy of 10 eV.

To obtain the thermal rate coefficient, the mutual neutralization cross section is fitted with a function of the form $\sigma(v) = Av^{-2} + Bv^{-1} + C + Dv$, where v is the relative collision velocity. By integrating $v\sigma(v)$ over an isotropic Maxwellian velocity distribution, a thermal rate coefficient of the form

$$\alpha(T) = A\left(\frac{2\mu}{\pi kT}\right)^{1/2} + B + 2C\left(\frac{2kT}{\pi\mu}\right)^{1/2} + \frac{3DkT}{\mu} \quad (4)$$

is obtained, where T is the temperature and k is the Boltzmann constant.

IV. RESULTS AND DISCUSSION

A. Effects of asymptotic forms of potentials

As discussed above, the asymptotic energy of the ion-pair state obtained from extrapolation of the calculated potential energy curves lies above the energy of the states $(3 - 5)^1\Sigma^+$, when it should be below. This will have an influence on the cross section, since the channels will be energetically open. In addition, the state $6^1\Sigma^+$ does not show the expected asymptotic behavior. Three calculations are carried out (referred to as calculation 1, 2 and 3 respectively) to assess the effect of this. In *calculation 1* the theoretical asymptotic energies that are given when extrapolating the calculated adiabatic potentials to large internuclear distances are used as threshold energies. In this calculation the ion-pair channel has a threshold energy that is the second highest relative the ground state threshold energy. In *calculation 2*, the last point ($R = 15$ a_0) of the adiabatic potential correlating to the ion-pair limit is changed so that the asymptotic energy would be the same relative to the state $3^1\Sigma^+$ as the experimental value in Table I. In *calculation 3*, data points beyond $R = 10$ a_0 of the adiabatic potential energies for the states $X^1\Sigma^+$ and $(2\text{-}5)^1\Sigma^+$ are removed. The experimental asymptotic energies (see Table I) are then used at the last point R = 15 a_0. The potential energy curves are then numerically interpolated between $R = 10$ a_0 and $R = 15$ a_0. The state $6^1\Sigma^+$ is assumed to show the correct behavior of a covalent potential up to around 6 a_0. The experimental asymptotic energy is then used at $R = 15$ a_0 and the potential is numerically interpolated between $R = 6$ a_0 and $R = 15$ a_0. The diabatization procedure is redone for each of the three calculations.

A comparison of the total mutual neutralization cross section for $H^+ + Cl^-$ obtained according to calculations 1, 2 and 3 is shown in Figure 4 for energies in the range of 1 meV to 10 eV . At low collision energies the mutual neutralization cross section has the $1/E$ behavior as expected from attractive Coulomb interactions [44]. At higher collision energies there are some structures in the calculated cross section. At smaller collision energies ($E < 3$ eV), calculation 1 gives a larger cross section than calculations 2 and 3. The asymptotic energy of the ion-pair channel is next highest relative to the ground state

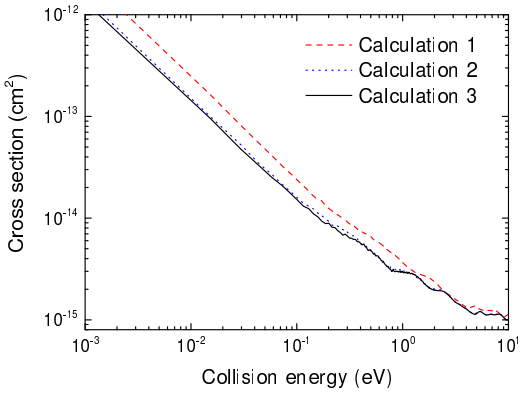

FIG. 4: (Color online) H^++Cl^- mutual neutralization cross sections obtained using the three different models of the asymptotic forms of the potential energy curves as described in the text.

energy in calculation 1 and therefore more channels are open at lower energies, which explains the larger cross section. At energies larger than about 17 eV all three cross sections almost entirely overlap. The cross sections obtained with calculations 2 and 3 are the same. Therefore, if the correct threshold energy of the ion-pair state is used, the calculation is not sensitive to the asymptotic behavior of the potentials. We chose calculation 3, where all asymptotic energies are the experimental values.

B. Effects of inclusion of closed channels

Using calculation 3 described above (with experimentally correct asymptotic limits), at low collision energies only the electronic ground state has a dissociation limit below the ion-pair limit. To study the effects of the inclusion of closed channel on the mutual neutralization cross section, the calculations are done by successively removing states, i.e., first removing the $6^1\Sigma^+$ state, then states 5 and $6^1\Sigma^+$ and so on until the calculation only included the ground and ion-pair states. In each case, the diabatization procedure is redone each time a state is removed.

Figure 5 shows the cross sections obtained by successively removing states from the calculation. At low collision energies (where the higher lying states are energetically closed) the inclusion of these states has a very small effect on the mutual neutralization cross section. At higher energies the calculations including fewer number of states start to provide a smaller mutual neutralization cross section. The most significant difference is achieved when the cross section is obtained using only two or three states. Including 6 coupled states, we believe the calculation of the mutual neutralization cross section is converged to a collision energy of about 10 eV.

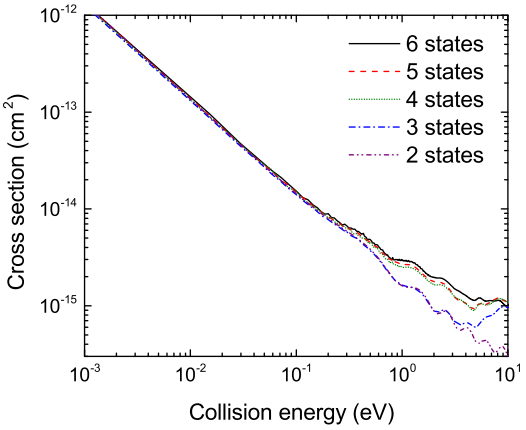

FIG. 5: (Color online) H^++Cl^- mutual neutralization cross section calculated by including different number of coupled states.

C. Final state distributions

From the quantum mechanical *ab initio* study, not only the total mutual neutralization cross section is obtained, but also the final state distributions. Figure 6 shows the computed final state distributions obtained using calculation 3. At low collisions only ground state fragments

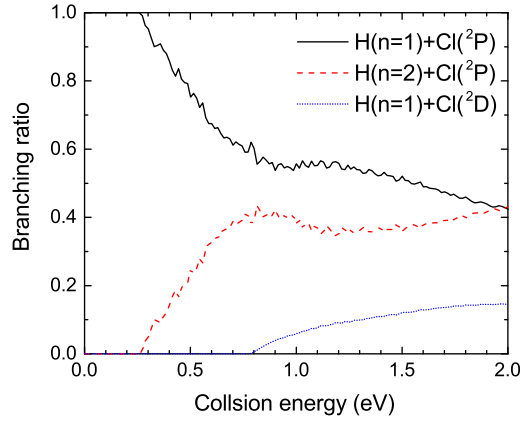

FIG. 6: (Color online) Final state distributions obtained using calculation 3 of H^++Cl^- mutual neutralization.

are formed. Above the threshold energy of H($n = 2$)+Cl, dissociation into this limit obtain a branching ration of about 50%. Also when states associated with H+Cl* become open for dissociation, these states start to contribute to the reaction. The flowing afterglow measurements [24] on the H^+/D^++Cl^- system is carried out at room temperature. We include all states up to an energy of 0.45 eV, where the H+Cl* limit opens up. Higher lying electronic states will not contribute in the experiment.

D. Effects of isotopic substitution

By changing the reduced mass of the collision complex, but assuming the potential energy curves and nonadiabatic coupling elements are the same for different isotopologues, the mutual neutralization reaction is studied for collisions of different isotopes of the hydrogen of chlorine ions. Figure 7 shows the calculated mutual neutralization cross sections for H^++$^{35}Cl^-$ and D^++$^{35}Cl^-$ using 6 coupled states (calculation 3). At low collision energies, the D^+ + Cl^- cross section is lower in magnitude than the cross section for H^+ + Cl^-. At higher collision energies (> 8 eV), the two cross sections become similar in magnitude. We have also computed the mutual neutralization cross section for collisions of H^++$^{37}Cl^-$, but since the very small difference in reduced mass, this cross section is found to be very close to the one of H^++$^{35}Cl^-$.

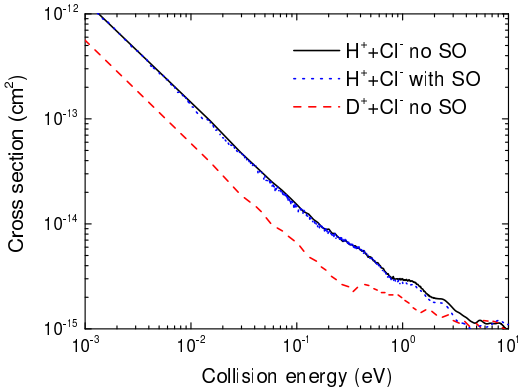

FIG. 7: (Color online) Mutual neutralization cross sections obtained using calculation 3 for collisions of H^++$^{35}Cl^-$ and D^++$^{35}Cl^-$. For H^++Cl^- the cross section calculated with and without inclusion of spin-orbit coupling is displayed.

E. Effects of spin-orbit interaction

By inclusion of the spin-orbit interaction by using the semi-empirical model [17, 18] described above in section III, the mutual neutralization cross section is computed by including all electronic states up to the H($n = 2$)+Cl(^2P) limit. These $\Lambda - S$ potentials for singlet and triplet states are displayed in Fig. 8 a) and b), respectively.

The electronic states associated with the H($n = 1$)+Cl(^2D) limit are not included in the model, since (as shown in Figure 5) theses states have minor importance for the mutual neutralization cross section. The cross section for mutual neutralization in collisions of H^++Cl^- calculated using the spin-orbit coupled Hamiltonian is displayed with the blue dotted curve in Figure 7 and as

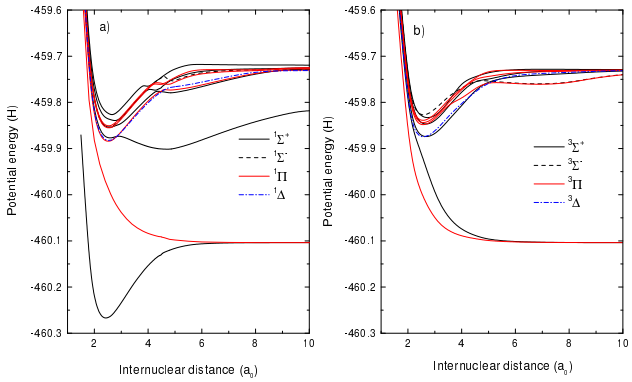

FIG. 8: (Color online) Adiabatic a) singlet and b) triplet states of HCl considered in the spin-orbit coupled Hamiltonian.

can be seen the inclusion of the spin-orbit interaction using this semi-empirical model has no effect on the mutual neutralization reaction.

F. Thermal rate coefficient

By fitting the mutual neutralization cross section with the formula given in section III, an analytical formula for the thermal rate coefficient according to equation (4) is obtained. The parameters of the fits of the H^++$^{35}Cl^-$ and D^++$^{35}Cl^-$ cross sections are given in Table IV. This provides thermal rate coefficient of H^++Cl^- of

TABLE IV: Parameters for fits of the mutual neutralization cross sections.

	A (cm^4s^{-2})	B (cm^3s^{-1})	C (cm^2)	D (cms)
H^++Cl^-	0.00257	$1.12 \cdot 10^{-9}$	$5.94 \cdot 10^{-16}$	$2.85 \cdot 10^{-23}$
D^++Cl^-	$5.67 \cdot 10^{-4}$	$1.03 \cdot 10^{-11}$	$1.02 \cdot 10^{-15}$	$1.08 \cdot 10^{-23}$

$\alpha\,(T = 300K) = 1.41 \cdot 10^{-8}$ cm^3s^{-1} and for D^++Cl^- it becomes $\alpha\,(T = 300K) = 4.15 \cdot 10^{-9}$ cm^3s^{-1}. These number should be compared with the measured values of $\alpha\,(T = 300K) = (3.2 \pm 1.0) \cdot 10^{-8}$ cm^3s^{-1} for H^++Cl^- and $\alpha\,(T = 300K) = (3.7 \pm 1.6) \cdot 10^{-9}$ cm^3s^{-1} for D^++Cl^- using the flowing afterglow-Langmuir probe experiment [24]. The measured rate coefficient of H^++Cl^- is a factor 2.6 larger than the calculated one. The measurement shows no significant isotope dependence in the rate coefficient, while the calculation provides a rate coefficient of the deuterated system that is smaller than the hydrogenated one. For several mutual neutralization processes [3, 4], the isotope effect is found to be very weak and the trend is that the collision complex with a larger reduced mass provides a slightly larger mutual neutralization cross section. The difference here is that the reaction is driven by non-adiabatic couplings at smaller internuclear distances among several states and the same scaling with the mass is not found.

G. Comparison with other systems and failure of the Landau-Zener model

In Figure 9, the calculated cross sections of H^+ + Cl^- mutual neutralization reactions are compared with those of H^++H^- [2, 3], He^++H^- [4], H^++F^- [9] and Li^++F^- [11]. As discussed in the introduction, the mutual neutralization reactions are in the case of H^++H− and He^++H− collisions driven by avoided crossings between ionic and covalent states occurring at large internuclear distances (> 30 a_0). For these systems at low collision energies many states are energetically open. The remaining systems H^++Cl^-, H^++F^- and Li^++F^- have in common that at low collision energies only the ground state is open for dissociation. The reaction is here driven by non-adiabatic interactions occurring at significantly smaller internuclear distances.

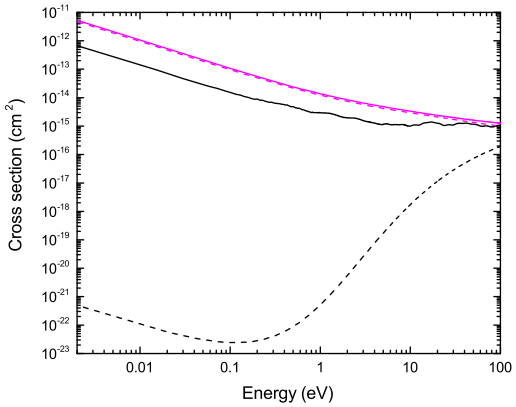

FIG. 9: (Color online) Calculated mutual neutralization cross sections for collisions of different atomic ions.

In the absorbing sphere model [45, 46] the mutual neutralization cross section can be approximated by $\sigma = \frac{\pi R_x}{E}$, where R_x is the internuclear distance where the electron is transferred from the ionic to covalent states. We note that the mutual neutralization cross sections for systems such as H^++H^- and He^++H^- are larger than the ones for collisions driven by avoided crossings at smaller internuclear distances.

The systems H^++Cl^-, H^++F^- and Li^++F^- might look similar when considering the change of character of the two lowest electronic states involved in the mutual neutralization reaction. However, the calculated mutual neutralization cross sections differ in many orders of magnitude. For both the H^++Cl^- and Li^++F^- reactions, the low energy cross sections show the $1/E$ depen-

dence and an effective formation of the ground state fragments. The cross section for formation of ground state fragments in the H^++F^- collisions is very small. The mutual neutralization cross section has a threshold when the H($n = 2$)+F channel opens up. This cross section is significantly smaller than the other ones and show clear resonant structures. (It should be noted, that in all studies except the H^++F^- study, strict diabatizations have been performed using *ab initio* calculated non-adiabatic coupling elements. For H^++F^-, quasi-diabatic electronic states were used [9].)

In several of the previous theoretical studies, not only quantum mechanical calculations have been performed, but also semi-classical Landau-Zener calculations [12, 13]. Provided reliable electronic couplings between the ionic and covalent states are applied, the semi-classical calculations often provide mutual neutralization cross sections that are in agreement with the fully *ab intio* quantum mechanical studies [3, 11, 15]. In collisions Li^++F^- it is found that the two-state Landau-Zener model works surprisingly well where it is assumed that involved crossing diabatic states coincide with the adiabatic states for internuclear distances smaller or larger than the region where the two states interact. The diabatic states can be obtained by an 2×2 orthogonal transformation of the adiabatic states, where the rotational angle of the transformation matrix is obtained by integrating the non-adiabatic coupling matrix $\alpha(R) = \int_R^{R_f} f_{12}(R')\, dR'$. To obtain this complete switch-over between the interacting states, this rotational angle should become $\pi/2$ when the internuclear distance is smaller than the distances where the two states interact. In the semi-classical study of Li^++F^- mutual neutralization [11], the non-adiabatic coupling element was scaled such that the rotational angle becomes $\pi/2$ at small internuclear distances. The calculated cross section was found to be very similar in magnitude and shape as the one obtained quantum mechanically as can be seen in Figure 10.

When a similar approach is applied in present system, there is a complete failure of the Landau-Zener model as can be seen in Figure 10. At low collision energies, the semi-classical cross section is orders of magnitude smaller than the one obtained quantum mechanically. This can be understood by a closer analysis of the interaction of the low-lying electronic states. The two lowest $^1\Sigma^+$ states of HCl interact over a relative large range of internuclear distances (see Figure 3). By integ..rating the f_{12} non-adiabatic coupling element over the region of the avoided crossing, $\pi/2$ is not obtained, but rather a value closer to π (3.32). This is an indication that in this region, not only the two lowest states interact but there are interactions in the same region among several states. By analyzing the dominant character of the MRCI wave function (see Figure 11), it can be seen that the ground state goes from being ionic at small internuclear distances to having a valence configuration at large distances as discussed by Bettendorff *et al.* [29], the double minimum of

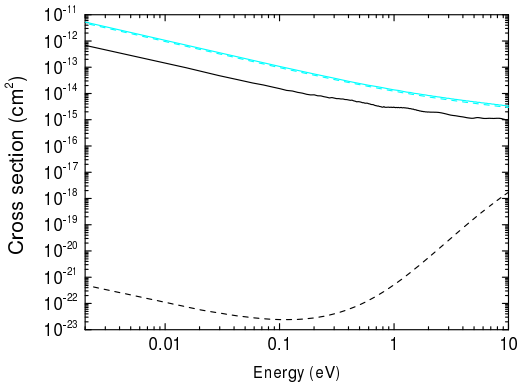

FIG. 10: (Color online) Mutual neutralization cross sections of Li^+ +F^- (cyan) and H^+ + Cl^- (black) calculated quantum mechanically (solid lines) and using the two-state Landau-Zener model (dashed)

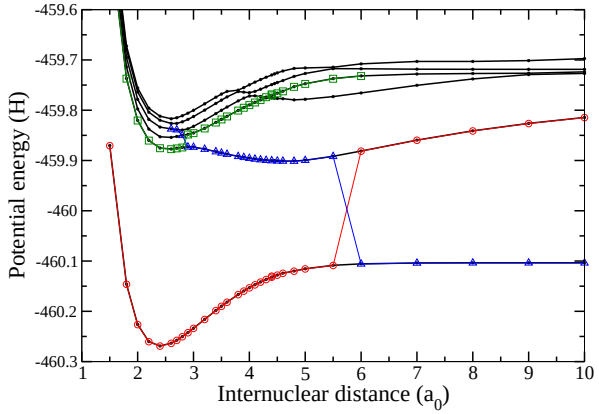

FIG. 11: (Color online) Adiabatic $^1\Sigma^+$ potential energy curves of HCl are shown with black curves. The red circles follow the state with a dominant configuration corresponding to the ion-pair state H^++Cl^-, while the blue triangles show the state dominated by a valence configuration and the green squares correspond to a Rydberg character.

the $2^1\Sigma^+$ state is a result of a change of character from Rydberg, to valence and then finally at large internuclear distances becoming the ion-pair state. Due to fact that several states simultaneously interact, the break-down of the Landau-Zener model is not particularly surprising. The effects of this mixing of the valence-Rydberg-ionic characters for the low-lying $^1\Sigma^+$ state of HCl have previously been discussed and analyzed by e.g., Lefebvre-Brion *et al.* [16].

The low-energy mutual neutralization cross section is larger for H^++Cl^- collisions than the cross section for D^++Cl^-. Also the corresponding thermal rate coefficient is larger for the system with the smaller reduced mass. This is in agreement with the approximate scaling relations of the ion-ion mutual neutralization rates

formulated by Hickman [46] and Miller [47], where the thermal rate scales with $\mu^{-0.5}$. A similar isotope effect of the mutual neutralization cross section was found from the *ab initio* quantum mechanical study of $Li^+ + H^-$ [5], where the $Li^+ + H^-$ cross section is larger than the neutralization cross section of $Li^+ + D^-$, while at higher collision energies the order is reversed. However, using both quantum mechanical as well as semi-classical Landau-Zener studies of mutual neutralization reactions such as $H^+ + H^-$ [3], $He^+ + H^-$ [4] it was found that at low energies the cross sections for the collision complex with the larger reduced mass produced a slightly larger magnitude. In the case of multi-state interactions, the simple scaling relations are not always valid.

V. CONCLUSIONS

We report quantum mechanical calculations on the mutual neutralization cross section for collisions of H^+ and Cl^- at energies less than 100 eV. The calculations are based on potential energy curves and non-adiabatic couplings among the six lowest $^1\Sigma^+$ states of HCl using the MRCI method. Although the reaction is driven by non-adiabatic interactions occurring at relative small internuclear distances, a sizable cross section is obtained. At low collision energies, only one state is open for dissociation. However, there is no isolated two-state avoided crossing driving the mutual neutralization reaction. There are simultaneous interactions between the ionic, valence and Rydberg states. For this system, two-state Landau-Zener model produce a mutual neutralization cross sections many orders of magnitude smaller than the quantal *ab initio* cross section. This shows the limitations of the Landau-Zener model when the reaction is driven by multi-state interactions occurring at relative small internuclear distances.

The calculated rate coefficient of $H^+ + Cl^-$ mutual neutralization has the same order of magnitude as the measured rate coefficient. The calculation shows a significantly stronger isotope dependence than what was found in the measurement. Since the experiment measures the sum of associative ionization and mutual neutralization direct comparison is not possible. In particular since for associative ionization interactions at small internuclear distances are important there may be a strong isotope effect. The calculation of associative ionization cross section is clearly needed. This is beyond the scope of this work and will be addressed in future study.

VI. SUPPLEMENTAL MATERIAL

Calculated adiabatic potential energy curves of the six lowest $^1\Sigma^+$ states of HCl are provided in atomic units as supplemental material. Also the non-adiabatic first-derivative coupling elements in among the same set of states can be found. This data is in atomic units and calculated for internuclear distances ranging between 1.5 and 15 a_0.

Acknowledgments

Å. L. acknowledges support from The Swedish Research Council.

[1] D. Fussen and C. Kubach, J. Phys. B: At. Mol. Opt. Phys. **19**, L31 (1986).
[2] M. Stenrup, Å. Larson, and N. Elander, Phys. Rev. A **79**, 012713 (2009).
[3] S. M. Nkambule, N. Elander, Å. Larson, J. Lecointre, and X. Urbain, Phys. Rev. A **93**, 032701 (2016).
[4] Å. Larson, S. M. Nkambule, and A. E. Orel, Phys. Rev. A **94**, 022709 (2016).
[5] H. Croft, A. S. Dickinson, F. X. Gadéa, J. Phys. B: At. Mol Opt. Phys. **32**, 81 (1999).
[6] A. S. Dickinson, R. Poteau, F. X. Gadéa, J. Phys. B: At. Mol Opt. Phys. **32**, 5451 (1999).
[7] A. K. Belyaev, P. S. Barklem, A. Spielfiedel, M. Guitou, N. Feautrier, D. S. Rodionov, and D. V. Vlasov, Phys. Rev. A, **85**, 032704 (2012).
[8] M. Guitou, A. Spielfiedel, D. S. Rodionov, S. A. Yakovleva, A. K. Belyaev, T. Merle, F. Thévenin, N. Feautrier, Chem. Phys. **462**, 94 (2015).
[9] J. Zs. Mezei, J. B. Roos, K. Shilyaeva, N. Elander, and Å. Larson, Phys. Rev. A **84**, 012703 (2011).
[10] S. Bienstock and A. Dalgarno, J. Chem. Phys. **78**, 224 (1983).
[11] S. M. Nkambule, P. Nurzia and Å. Larson, Chem. Phys. **462**, 23 (2015).
[12] L. Landau, Phys. Z. Sowjetunion **2**, 46 (1932).
[13] C. Zener, Proc. R. Soc. London Ser. A **137**, 696 (1932).
[14] A. K. Belyaev, P. S. Barklem, A. S. Dickinson, and F. X. Gadéa, Phys. Rev. A **81**, 032706 (2010).
[15] H. M. Hedberg, S. Nkambule, and Å. Larson, J. Phys. B: At. Mol. Opt. Phys **47**, 22 (2014).
[16] H. Lefebvre-Brion, H. P. Liebermann, and G. J. Vázquez, J. Chem. Phys. **134**, 204104 (2011).
[17] J. S. Cohen, B. Schneider, J. Chem. Phys. **61**, 3230 (1974).
[18] P. J. Hay, T. H. Dunning, R. C. Raffenetti, J. Chem. Phys. 65, 2679 (1976).
[19] H. T. Schmidt *et al.*, Review Scientific Instruments **84**, 055115 (2013).
[20] B. Peart and D. A. Hayton, J. Phys. B: At. Mol. Opt. Phys. **25**, 5109 (1992).
[21] T. Nzeyimana, E. A. Naji, X. Urbain, and A. Le Padellec, Eur. Phys. J. D **19**, 315 (2002).
[22] R. F. Nascimento, N. de Ruette, A. Dochain, M. Kaminska, M. H. Stockett, H. T. Schmidt, H. Cederquist, and X. Urbain, X, J. Phys. Conf. Ser. **635**, UNSP 022043 (2015).
[23] N. S. Shuman, T. M. Miller, R. Johnsen, and A. A. Viggiano, J. Chem. Phys. **140**, 044304 (2014).
[24] J. C. Sawyer, T. M Miller, B. C. Sweeny, S. G. Ard, A. A. Viggiano, and N. S. Shuman, J. Chem. Phys. **149**, 044303 (2018).
[25] Å. Larson, S. Fonseca dos Santos, and A. E. Orel, J. Chem. Phys., **147**, 084304 (2017).
[26] MESA (Molecular Electronic Structure Applications) (1990) P. Saxe, B. H. Lengsfield, R. Martin and M. Page.
[27] A. D. McLean and G. S. Chandler, J. Chem. Phys., **72**, 5639, (1980).
[28] D. M. Hirst and M. F. Guest, Mol. Phys., **41**, 1483, (1980).
[29] M. Bettendorff, S. D. Peyerimhoff, and R. J. Buenker, Chem. Phys. **66**, 261, (1982).
[30] S. Engin, N. Sisourat, and S. Camiato, Chem. Phys., **137**, 154304 (2012).
[31] Transport Properties of Ions in Gases, E. A. Mason, and E. W. McDaniel, John Wiley & Sons (1988).
[32] A. Kramida, Y. Ralchenko, J. Reader, and NIST ASD Team (2016). Nist atomic spectra database (version 5.4), [online]. available: http://physics.nist.gov/asd.
[33] "Constants of Diatomic Molecules" by K.P. Huber and G. Herzberg (data prepared by J.W. Gallagher and R.D. Johnson, III) in NIST Chemistry WebBook, NIST Standard Reference Database Number 69, Eds. P.J. Linstrom and W.G. Mallard, National Institute of Standards and Technology, Gaithersburg MD, 20899, doi:10.18434/T4D303.
[34] B. H. Lengsfield III and D. R. Yarkony, Adv. Chem. Phys. **82**, 1 (1992).
[35] B. H. Lengsfield III, P. Saxea, and D. R. Yarkony, J. Chem. Phys., **84**, 4549 (1984).
[36] J. Hellmann, Einfohrung in die Quantenchemie (Deuticke, Leipzig, 1937).
[37] R. P. Feynmann, Phys. Rev. **56**, 340 (1939).
[38] V. Sidis, J. Chern. Phys. bf 55, 5838 (1971).
[39] W. D. Hobey and A. D. McLachlan, J. Chem. Phys. **33**, 1695 (1960).
[40] F. T. Smith, Phys. Rev. **179**, 111 (1969).
[41] C. A. Mead and D. G. Truhlar, J. Chem. Phys. **77**, 6090 (1982).
[42] A. Kramida, Y. Ralchenko and J. Reader, NIST Atomic Spectra Database (ver 5.3), [Online]. Available: http://physics.nist.gov/asd [2018, April 1]. (National Institue of Standards and Technology, Gaithersburg, MD, 2018).
[43] B. R. Johnson, J. Comp. Phys. **13**, 445 (1973).
[44] E. P. Wigner, Phys. Rev. **73**, 1002 (1948).
[45] R. E. Olson, J. Chem. Phys. **56**, 2979 (1972).
[46] A. P. Hickman, J. Chem. Phys. **70**, 4872 (1979).
[47] T. M. Miller, J. Chem. Phys. **72** 4659 (1980).